

Characteristics of anodic TiO₂ nanotube arrays mediated IrO₂ Active Anode in the Oxygen Evolution Reaction

Huazhen Cao^{*}, Lingqin Zhang, Mengjie Chen

College of Materials Science and Engineering, Zhejiang University of Technology, Hangzhou 310014, China,

*E-mail: caohz@zjut.edu.cn

Received: 4 January 2022 / Accepted: 22 February 2022 / Published: 4 March 2022

Herein, we report a simple approach for the synthesis of a high-performance and structurally stable IrO₂ active anode for the oxygen evolution reaction. To summarize, anodic TiO₂ nanotube arrays (TNTs) were grown on Ti substrate and then active IrO₂ was decorated over the regular TNTs/Ti by electrodeposition and heat treatment. The effects of the TNTs as well as the preparation conditions, such as the deposition charge of IrO₂ and the calcination temperature, were discussed intensively. The TNTs provide a beneficial spatial structure for the growth of active IrO₂, which ensures the desired electrocatalytic activity and adaptability of an electrode for long-term use in the oxygen evolution reaction. The electrochemical surface structure of this novel OER anode was investigated by cyclic voltammetry studies. Both the "external" and "internal" active sites could well exert their effects when the deposition charge of IrO₂ was controlled at an optimal value (500 mC), and a high porosity was obtained in this case, which is most conducive to proton exchange. In addition, the calcination temperature also played an important role in the electrode performance because the nanostructure of the TNTs are destroyed at high temperatures.

Keywords: IrO₂ active anode, Interlayer, Oxygen evolution, Electrochemical surface structure, Catalytic properties

1. INTRODUCTION

The oxygen evolution reaction (OER) is critical for converting and storing clean energy [1,2]. The OER, however, is a dynamically slow process that significantly limits energy conversion efficiency [3,4]. Therefore, great attention has been given to developing an efficient OER electrocatalyst. It is currently known that RuO₂ is the most active electrocatalytic coating for the oxygen evolution reaction, but the RuO₂/Ti anode has poor stability at high potentials, which limits its application in this regard [5,6]. As a catalyst second only to RuO₂ in acid solution, IrO₂ has a low oxygen evolution overpotential and a service life approximately 20 times larger than that of RuO₂ [7-10]. Therefore, IrO₂ is widely used

in electroplating, electrometallurgy, organic degradation, and other industrial fields [11-13]. Although the IrO₂ coating itself is relatively stable, cracks usually exist on the surface when the coating is prepared in a traditional way. The electrolyte easily contacts the titanium substrate through the cracks, causing the dissolution and oxidation of the titanium substrate and resulting in the generation of nonconductive TiO₂, which leads to the stripping of the active layer and a sharp decrease in OER activity.

In recent years, many processes have been developed to solve the abovementioned electrode deactivation problem. Incorporation of inert components into the active layer is a commonly used method. For example, Herrada et al. [14] studied IrO₂-Ta₂O₅/Ti coatings with different molar ratios, and the accelerated life was increased by 22 times by selecting an optimum composition. However, inert oxides inevitably affect the electrochemical activity of active oxides, since they do not show electrochemical activity. In addition, the conductivity of a coated electrode will decrease with the addition of inert components.

Anodic TiO₂ nanotube arrays (TNTs) possess highly a ordered three-dimensional structure, large specific surface area, smooth charge transfer path and good stability; in particular, the crystalline TNTs can exhibit lower resistivity than a non-conductive TiO₂ layer generated over time [15-17]. Therefore, TNTs are an ideal intermediate layer between the titanium base and IrO₂. They can not only ensure good conductivity of the coating but also endow the active component with good binding strength, which is favorable for improving the stability of coated electrodes.

In this work, we introduce a new method for decorating granular IrO₂ over regular TNTs/Ti by the electrodeposition method, as it has some unique advantages, especially the grain size of the active material, which can be controlled by adjusting the deposition potential or current density [18,19]. Moreover, noble metal oxide coatings prepared by the electrodeposition method are characterized by low cost, high efficiency and strong stability, which have great industrial application prospects and can allow the realization of mass production [20]. Based on measurements of cyclic voltammetry (CV) and chronoamperometry (CA), it is revealed that the TNTs-mediated iridium oxide electrode has vigorous catalytic activity and stability for the OER. The electrochemical surface structure of this novel OER anode was also investigated in detail.

2. EXPERIMENTAL

2.1. Preparation of IrO₂/TNTs/Ti electrodes

Titanium sheets (1.5×2 cm²) were pretreated in an aqueous solution containing 75 g L⁻¹ CrO₃ and 4 wt% HF at 50 °C for 20 min. After washing and drying, anodic oxidation was carried out in an electrolyte of 1 wt% HF with a titanium sheet as the anode and a graphite electrode as the cathode. The anodic oxidation voltage was 20 V, the reaction time was 20 min, and the temperature was kept at 25 °C. The anodized TNTs samples were heat treated at 450 °C for 2 h in an air atmosphere. After cooling in the furnace, the TNTs in the amorphous state could be transferred to the anatase phase [21].

The granular IrO₂ was decorated onto the TNTs by electrochemical deposition. H₂IrCl₆·6H₂O was dissolved in deionized water. After mixing evenly, 5 g L⁻¹ H₂C₂O₄ and 10 g L⁻¹ H₂O₂ were added

successively. The pH value of the deposition solution was adjusted to 10.5, and the iridium concentration was controlled at 2 mmol L^{-1} . In a three-electrode system, TNTs were used as the working electrode, platinum was used as the counter electrode, and a saturated calomel electrode was used as the reference electrode. In the above solution, -0.05 mA cm^{-2} galvanostatic deposition was performed on the TNTs. We studied the effects of different deposition charges (100 mC, 300 mC, 500 mC and 700 mC) on the OER. The results showed that the electrode prepared with a deposition charge of 500 mC had the best oxygen evolution performance. After that, the deposited samples were placed in a tubular furnace and calcined at the selected temperatures (350°C , 450°C , 550°C , 650°C) for 1 h and then cooled within the furnace to obtain the $\text{IrO}_2/\text{TNTs}/\text{Ti}$ electrodes. As a comparison, a IrO_2/Ti electrode without TNTs was also prepared by directly electrodepositing IrO_2 with a deposition charge of 500 mC on Ti in the above solution and calcining at 450°C .

2.2. Physical characterization and electrochemical measurements

The phases of the samples were characterized by X-ray diffraction (XRD, Panalytical X'Pert PRO, $\text{Cu K}\alpha \lambda = 0.154 \text{ nm}$). The surface morphologies of the electrodes were observed with a scanning electron microscope (SEM, Energy Dispersion X-ray Spectrum) operating at 5-20 kV. All electrochemical tests were carried out in a three-electrode system on a CHI660c electrochemical workstation. A Pt electrode and a saturated calomel electrode were used as the counter electrode and reference electrode, respectively, and the prepared samples were used as working electrodes. Cyclic voltammetry was performed to study the active surface structure of the electrodes. The potential scanning range was 0-1.2 V with a scanning rate of 20 mV s^{-1} in $0.5 \text{ mol L}^{-1} \text{ H}_2\text{SO}_4$ solution. The polarization curves were measured at a scanning rate of 1 mV s^{-1} in $0.5 \text{ mol L}^{-1} \text{ H}_2\text{SO}_4$ solution. The oxygen evolution catalytic activity of each electrode was studied by measuring the initial oxygen evolution potential and the current response density at the same potential. The stability of each $\text{IrO}_2/\text{TNTs}/\text{Ti}$ electrode with regard to the OER was studied in $1 \text{ mol L}^{-1} \text{ H}_2\text{SO}_4$ system by chronoamperometry at 40°C with an applied potential of 1.5 V.

3. RESULTS AND DISCUSSION

3.1. XRD analysis

Fig. 1 shows the XRD patterns of the $\text{IrO}_2/\text{TNTs}/\text{Ti}$ electrodes before and after calcination. A weak diffraction peak of the TNTs intermediate layer is observed at $2\theta = 25.2^\circ$. For the untreated specimen, there only exists a soft IrO_2 characteristic peak located at $2\theta = 34.7^\circ$, which demonstrates that the IrO_2 was not completely crystallized. After calcination, three strong characteristic peaks emerge at $2\theta = 28.0^\circ$, 34.7° and 53.9° , denoting the existence of anatase IrO_2 [22]. XRD analysis reveals that the active oxide IrO_2 prepared by electrodeposition is amorphous, and heat treatment can cause the transformation of the active oxide IrO_2 coating from an amorphous state to a crystalline state to obtain a stable structure.

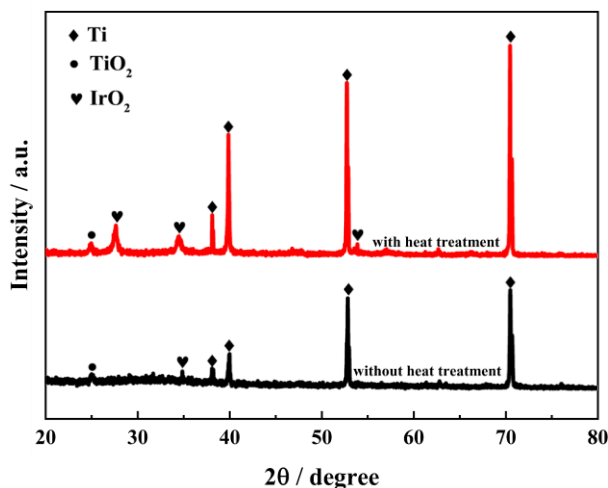


Figure 1. XRD patterns of $\text{IrO}_2/\text{TNTs}/\text{Ti}$ electrodes calcined at $450\text{ }^\circ\text{C}$ with a deposition charge of 500 mC and without heat treatment.

3.2. Morphological observation

To study the electrodeposition process of granular IrO_2 on TNTs, a series of scanning electron microscope images for the samples prepared under different deposition charges are gathered, as shown in Fig. 2. Fig. 2a-d shows the surface morphologies of $\text{IrO}_2/\text{TNTs}/\text{Ti}$ electrodes calcined at $450\text{ }^\circ\text{C}$ with deposition charges of 100, 300, 500 and 700 mC, respectively. From the surface morphology of the electrode with a deposition charge of 100 mC (Fig. 2a), the nanostructured TNTs are clearly observed, and only a few particles grow into the nanotubes. As the electrodeposition proceeds (Fig. 2b), the voidage of nanotubes decreases due to the growth of the IrO_2 particles along the tube walls of the TNTs. The structures of the TiO_2 nanotubes can still be clearly observed when the deposition charge is 300 mC. When the deposition charge increases to 500 mC (Fig. 2c), the active oxide IrO_2 accumulates in the shape of granular particles with a size of approximately 40 nm, which cover the TNTs, and the interstice is still visible. Fig. 2d shows the morphology of the sample with a deposition charge of 700 mC. The accumulated particles of active oxide IrO_2 grow further and connect together to form a compact layer. The TNTs intermediate layer is almost completely covered, displaying a reduced specific surface area compared to the other samples. For comparison, the IrO_2/Ti electrode prepared by the same electrodeposition method was also characterized. Fig. 2e shows the surface micromorphology of IrO_2/Ti with a deposition charge of 500 mC. The IrO_2/Ti electrode (Fig. 2e) without TNTs interlayer presents a compact structure with large IrO_2 particles on the surface.

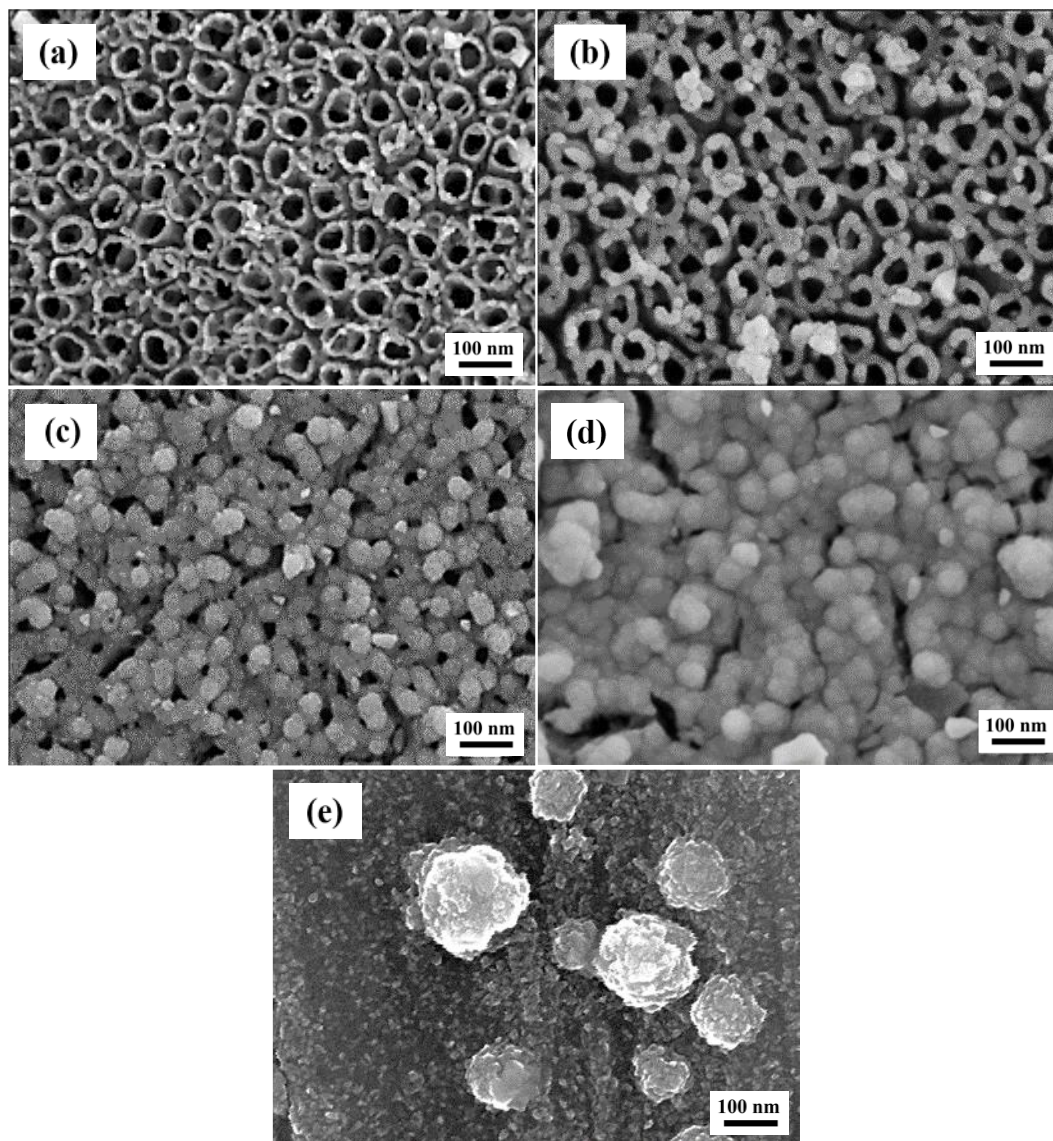


Figure 2. SEM images of IrO₂/TNTs/Ti electrodes with IrO₂ deposition charges of (a) 100 mC, (b) 300 mC, (c) 500 mC, (d) 700 mC (calcination temperature: 450 °C) and (e) IrO₂/Ti electrodes.

Fig. 3 displays the surface morphologies of the IrO₂/TNTs/Ti electrodes under different calcination temperatures. In this series of experiments, the IrO₂ deposition charge was kept at 500 mC. It is found that for the sample calcined at 350 °C, the packed IrO₂ is loosely distributed in the interspace of the TNTs without a definite shape. When the calcination temperature is increased to 450 °C (Fig. 2c), granular IrO₂ nanoparticles are formed that grow along the tube walls of the TiO₂. The specimen calcined at 450 °C presents a regular microporous structure with a large surface area. However, a higher calcination temperature (≥ 550 °C) will induce the production of whiskers (Fig. 3b), and the whiskers develop rapidly with increasing temperature (Fig. 3c). Furthermore, these active IrO₂ particles tend to grow into coarse grains at higher calcination temperatures and are unevenly distributed on the electrode surface. There are disadvantages to this structure; for example, the poor bonding strength between IrO₂ and the TNTs interlayer easily results in local exfoliation. From the SEM observation, the sample

calcined at 450 °C has an optimum structure; the active oxides are uniformly distributed, and this embedded spatial structure seems more stable.

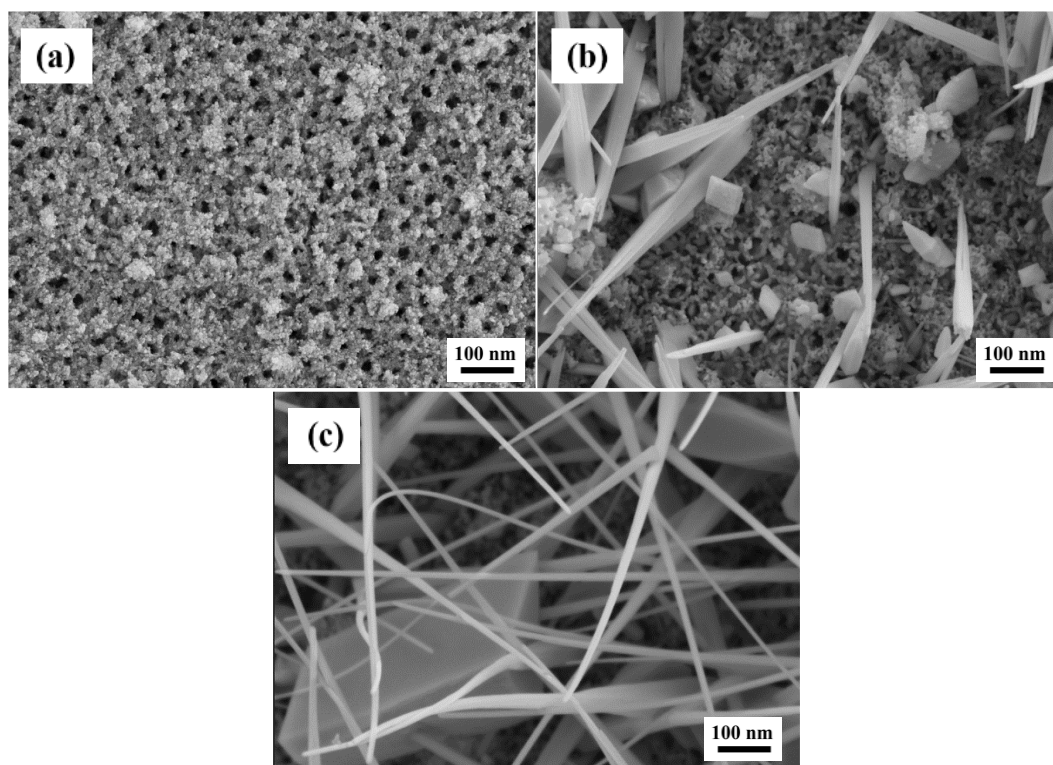


Figure 3. SEM images of IrO₂/TNTs/Ti electrodes calcined at (a) 350 °C, (b) 550 °C, and (c) 650 °C, with an IrO₂ deposition charge of 500 mC.

3.3. Polarization curves

Fig. 4 shows the polarization curves of the IrO₂/Ti electrode without TNTs intermediate layer (IrO₂/Ti), the IrO₂/TNTs/Ti electrode calcined at 450°C with a deposition charge of 500 mC, and the IrO₂/TNTs/Ti electrode with a deposition charge of 500 mC and without heat treatment. The catalytic activities of the IrO₂ coated electrodes for the OER in 0.5 mol L⁻¹ H₂SO₄ solution are studied by the measurement of polarization curves. For all samples, the initial potential of oxygen evolution is approximately 1.3 V. Comparing the polarization curves of IrO₂/Ti and IrO₂/TNTs/Ti with or without calcination, the result shows that the response current density of the IrO₂/TNTs/Ti electrode with calcination is much higher than that of the electrode without calcination. As identified by XRD analysis (Fig. 1), the amorphous active oxide can be transformed to a crystalline state by calcination. Therefore, it can be concluded that anatase IrO₂ has a better electrocatalytic activity for the evolution of oxygen. In addition, it is also noted that the response current density increases considerably by the introduction of TNTs; that is, the TNTs interlayer plays a positive role in the activity of the IrO₂ coating electrode. In addition, some typical electrodes were investigated (Table 1). The IrO₂/TNTs electrodes prepared have a current density of approximately 28 mA cm⁻² at -1.4 V. Compared with single hydrogen-doped anatase

titanium dioxide (H:TiO₂) [23] and IrO₂ [24], the IrO₂/TNTs electrodes have better oxygen evolution activity. Genova-Koleva et al. [24] synthesized TNTs by a modified hydrothermal method, and the supported (50 wt%) IrO₂ catalyst was synthesized by hydrolysis of its chlorides in alkaline media. The Nb-TiO₂ supported IrO₂ catalyst (IrO₂/Nb_{0.05}Ti_{0.95}O₂) was prepared by a modified colloidal method [25]. In this paper, TNTs were prepared by anodic oxidation, and IrO₂ was loaded by constant current deposition. The oxygen evolution performance of the IrO₂/TNTs electrodes prepared by this method were better than those of the aforementioned previously reported electrodes.

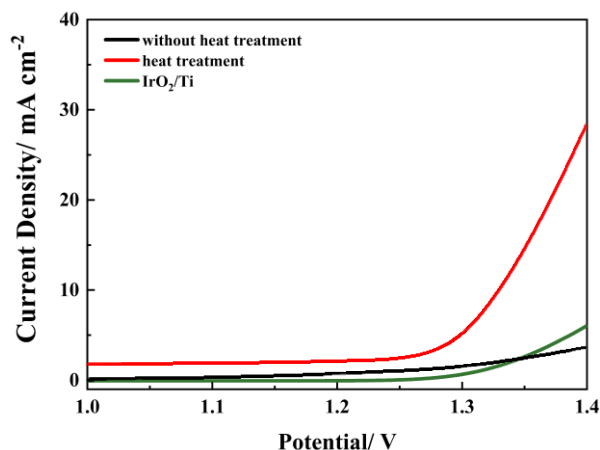


Figure 4. Polarization curves of the IrO₂/Ti electrode without TNTs intermediate layer (IrO₂/Ti), IrO₂/TNTs/Ti electrode calcined at 450°C with a deposition charge of 500 mC, and IrO₂/TNTs/Ti electrode with a deposition charge of 500 mC and without heat treatment, measured at a scanning rate of 1 mV s⁻¹ in 0.5 mol L⁻¹ H₂SO₄ solution.

Table 1. Current densities from the polarization curves of investigated electrodes.

Electrodes	Preparation method	Current density	Experimental parameters
H:TiO ₂ [23]	RF-magnetron sputtering	1.8 mA cm ⁻² (potential: 1.4 V)	in 1 mol L ⁻¹ KOH solutions
IrO ₂ [24]	thermal decomposition method	21 mA cm ⁻² (potential: 1.55 V)	scan rate: 5 mV s ⁻¹ ; in 0.5 mol L ⁻¹ H ₂ SO ₄
IrO ₂ /TNTs [24]	TNTs: hydrothermal method IrO ₂ /TNTs: hydrolysis of chlorides	5 mA cm ⁻² (potential: 1.5 V)	scan rate: 20 mV s ⁻¹ ; in 0.1 mol L ⁻¹ KOH
IrO ₂ /Nb _{0.05} Ti _{0.95} O ₂ [25]	modified colloidal method	17 mA cm ⁻² (potential: 1.55 V)	scan rate: 5 mV s ⁻¹ ; in 0.5 mol L ⁻¹ H ₂ SO ₄

3.4. Cyclic voltammetric characteristics

Fig. 5 shows the cyclic voltammetry curves of IrO₂ electrodes prepared under different conditions. The IrO₂/Ti electrode with particles directly deposited onto a Ti plate is relatively coarse and shows poor adhesion, which leads to a weak current response for the OER. For the IrO₂/TNTs/Ti electrodes, there exists one wide oxidation peak in their cyclic voltammetry curves, which corresponds

to the valence state transition of iridium by proton exchange with the electrolyte on the electrode surface [26]. In Fig. 5a, the response current density shows an increasing trend with increasing deposition charge. That is, to some extent, the amount of iridium oxide may affect the amount of surface active sites that exchange protons with the electrolyte in the same system. When the deposition charge exceeds 500 mC, the influence of the IrO_2 deposition content is comparatively not significant, and the increasing tendency of the response current slows down. Therefore, considering the electrode properties and cost factors, the appropriate amount of IrO_2 is obtained when conducting galvanostatic deposition for 500 mC at a current density of -0.05 mA cm^{-2} .

The cyclic voltammetry curves in Fig. 5b indicate that calcination temperature is particularly important for this nanostructured electrode. It is found that the IrO_2 electrodes almost lose activity under high calcination temperatures (e.g., $550 \text{ }^\circ\text{C}$, $650 \text{ }^\circ\text{C}$), and the current responses of these electrodes are very weak in the testing range of 0-1.2 V. The performance deterioration at higher temperatures may be related to their structural change, as identified by SEM characterization (Fig. 3). In addition, despite the many advantages of TNTs, a high calcination temperature will cause the collapse of TiO_2 nanotube arrays [27], and the destruction of the nanostructure adversely affects the surface reaction. The sample electrode calcined at $450 \text{ }^\circ\text{C}$ has a regular nanostructure and high crystallinity, which endows it with the desired performance, i.e., high electrocatalytic activity and excellent stability. However, using too low of a temperature during heat treatment will lead to incomplete crystallization. Therefore, the cyclic voltammetry curve of the $\text{IrO}_2/\text{TNTs}/\text{Ti}$ electrode calcined at $350 \text{ }^\circ\text{C}$ shows a different shape; the anodic current is inferior to that of the electrode calcined at $450 \text{ }^\circ\text{C}$, and the reduction peak has an obvious shift compared to those of the other samples.

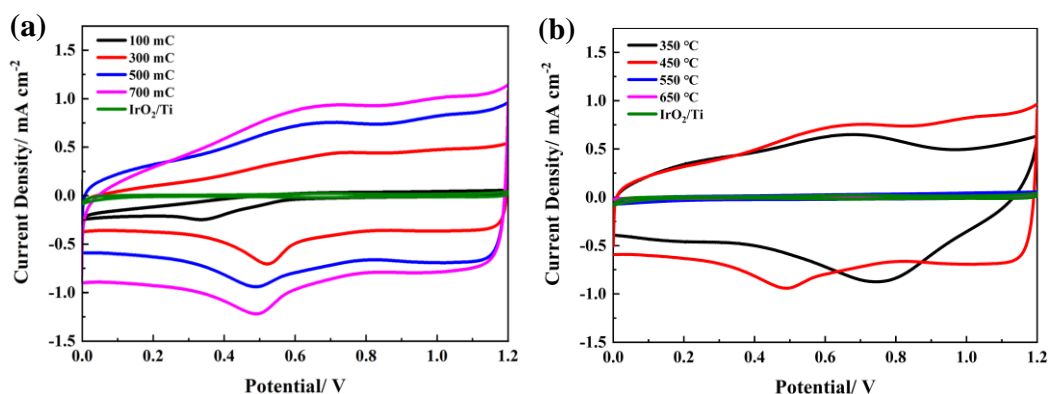


Figure 5. Cyclic voltammetry curves of IrO_2/Ti and $\text{IrO}_2/\text{TNTs}/\text{Ti}$ electrodes with (a) different IrO_2 deposition charges (calcination temperature: $450 \text{ }^\circ\text{C}$) and (b) different calcination temperatures (deposition charge: 500 mC) in $0.5 \text{ mol L}^{-1} \text{ H}_2\text{SO}_4$ solution at a scanning rate of 20 mV s^{-1} .

The cyclic voltammetry integral charge q , a key parameter reflecting the number of surface active sites, is derived by integrating the cyclic voltammetry curves in Fig. 5. From the q values of the different $\text{IrO}_2/\text{TNTs}/\text{Ti}$ electrodes (Table 2), we can clearly see the increasing trend of integral charge when increasing the deposition charge. When the deposition charge exceeds 500 mC, its influence on the integral charge is reduced. To obtain the quantitative relationship between the deposition charge and the

q value, the ratio of the q value to the deposition charge is defined as the number of active sites of a $\text{IrO}_2/\text{TNTs}/\text{Ti}$ electrode under the same deposition charge (Fig. 6):

$$q^* = q / Q \quad (1)$$

Table 2 The values of q for $\text{IrO}_2/\text{TNTs}/\text{Ti}$ electrodes with different IrO_2 deposition charges (calcination temperature: 450 °C; measured at scanning rate of 20 mV s^{-1} in 0.5 mol L^{-1} H_2SO_4 solution).

	100 mC	300 mC	500 mC	700 mC
$q/\text{mC cm}^{-2}$	9.68	43.4	77.85	96.07

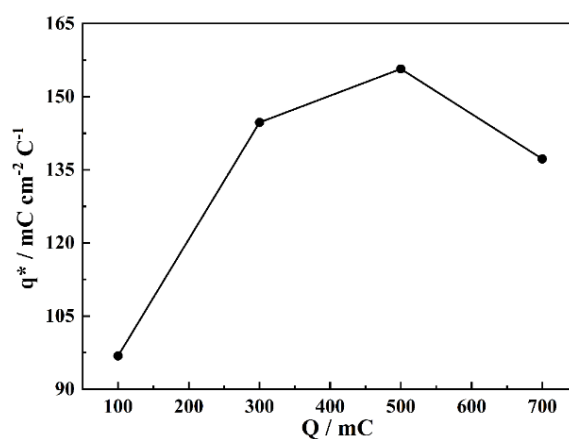


Figure 6. Value of q^* for $\text{IrO}_2/\text{TNTs}/\text{Ti}$ electrodes with different IrO_2 deposition charges (calcination temperature: 450 °C; measured at scanning rate of 20 mV s^{-1} in 0.5 mol L^{-1} H_2SO_4 solution).

Fig. 6 shows that the q^* value does not increase monotonously with increasing deposition charge; it reaches an optimal value when the deposition charge reaches 500 mC. In the initial stage of deposition, with an increase in deposition charge, an active oxide will preferentially attach to the tube walls of the TNTs, so the surface active sites will increase with the increase in the active components. As deposition progresses, the active component will aggregate into large particles and accumulate on the surface of the TNTs nanotubes; then, some active substances will be covered and will not exert their effects. Therefore, the q^* value decreases when the deposition power exceeds 500 mC.

Table 3 The values of q for $\text{IrO}_2/\text{TNTs}/\text{Ti}$ electrodes prepared under different calcination temperatures. (deposition charge: 500 mC; measured at scanning rate of 20 mV s^{-1} in 0.5 mol L^{-1} H_2SO_4 solution)

	350 °C	450 °C	550 °C	650 °C
$q/\text{mC cm}^{-2}$	59.96	77.85	3.08	0.88

Table 3 displays the integral charge q values of electrodes prepared with different calcination temperatures. The difference in the q values is dramatic, especially for the samples calcined at 550 °C and 650 °C, and a low q value denotes fewer active sites and thus poor electrocatalytic activity.

3.5. Electrochemical surface structure

Cyclic voltammetry tests were carried out on the IrO₂/TNTs/Ti electrodes at different scanning rates. The relationship between the cyclic voltammetry integral charge q and scanning rate ν is obtained. When ν increases, proton exchange between the solution and the "internal" active surface is very difficult because the solution needs to pass through the active oxide gap and crystal interface. The q value will decrease with increasing ν [28]. At this time, the proton exchange between the solution and the electrode only occurs on the "outer" active surface of the electrode [29]. When ν is very small, both the "outer" active surface of the electrode and the "internal" active surface, which is difficult to reach, can exchange protons with the solution. For the quantitative calculation of cyclic voltammetric charge on the "external" and "internal" active surfaces of the electrode, Ardizzone and Trasatti [30] proposed the following two linear formulas:

$$1/q = 1/(q_{inner} + q_{outer}) + C_1 \nu^{1/2} \quad (2)$$

$$q = q_{outer} + C_2 \nu^{-1/2} \quad (3)$$

where q_{outer} is related to the "outer" active surface of the electrode, and q_{inner} is related to the "inner" active surface of the electrode. The sum of q_{inner} and q_{outer} is defined as q_{total} .

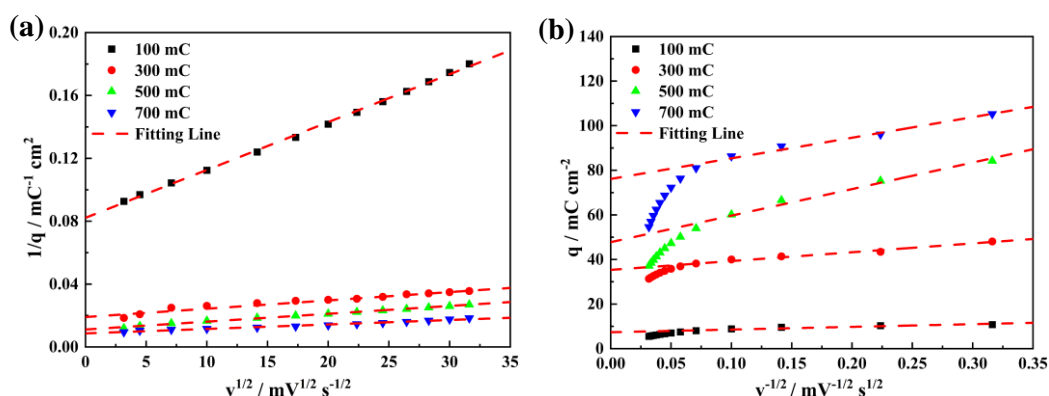


Figure 7. Extrapolation of integrated voltammetric charge q for IrO₂/TNTs/Ti electrodes with different IrO₂ deposition charges (calcination temperature: 450 °C; measured at scanning rate of 20 mV s⁻¹ in 0.5 mol L⁻¹ H₂SO₄ solution), to (a) $\nu \rightarrow 0$ and (b) $\nu \rightarrow \infty$. Dashed line: linear fitting.

According to the linear Formulas (2) and (3), the functions $1/q \cdot \nu^{1/2}$ and $q \cdot \nu^{-1/2}$ are plotted, which are shown in Fig. 7. We know that when $\nu \rightarrow 0$, $q = q_{total}$ and when $\nu \rightarrow \infty$, $q = q_{outer}$, thus we can obtain q_{inner} . As shown in Fig. 7a, the curves maintain a good linear relationship in most scanning speed ranges. Fig. 7b shows that there is a fast drop in the q value at a high scanning rate for the sample electrode with

a larger deposition charge. Despite the greater amount of active sites in this sample electrode, the proton exchange between the solution and the surface active oxide is incomplete over a short reaction time, which results in this phenomenon.

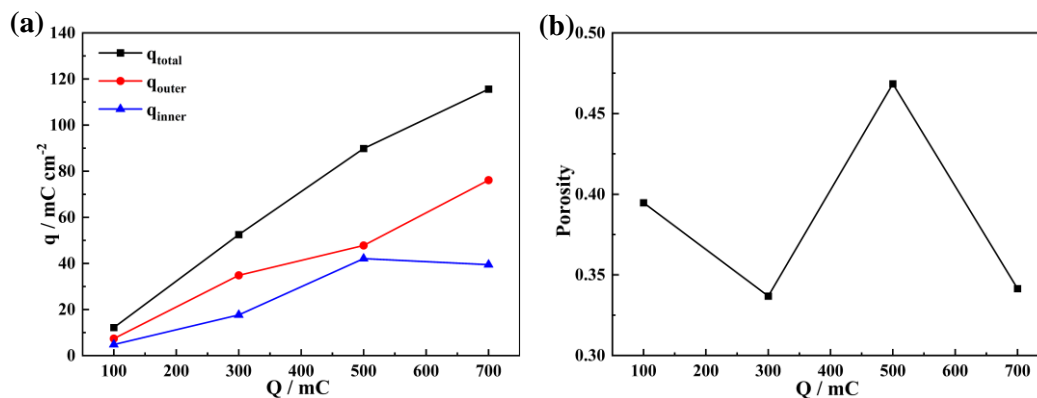


Figure 8. Values of (a) q_{inner} , q_{outer} , q_{total} and (b) porosity of the $\text{IrO}_2/\text{TNTs}/\text{Ti}$ electrodes with different IrO_2 deposition charges (calcination temperature: $450\text{ }^\circ\text{C}$) as a function of deposition charge (measured at a scanning rate of 20 mV s^{-1} in $0.5\text{ mol L}^{-1}\text{ H}_2\text{SO}_4$ solution).

Fig. 8a shows the q_{inner} , q_{outer} and q_{total} values of the $\text{IrO}_2/\text{TNTs}/\text{Ti}$ as a function of IrO_2 deposition charge. q_{outer} and q_{total} both present an increasing trend with increasing IrO_2 deposition charge, while q_{inner} reaches a maximum value at a deposition charge of 500 mC and then decreases. As identified by SEM observation, when the deposition charge is less than 500 mC , the ordered nanometer array structure can be well preserved, which is favorable for proton exchange between the inner active substance and the solution. However, overdeposition, e.g., a deposition charge of 700 mC , will lead to the nanotube structure being completely covered. In this case, the solution has difficulty penetrating the inner side, thus reducing the "inner" surface active sites.

The ratio of q_{inner} to q_{total} is used to define the electrochemical porosity,

$$\varphi = q_{inner} / q_{total} \quad (4)$$

Fig. 8b displays the electrochemical porosity of the $\text{IrO}_2/\text{TNTs}/\text{Ti}$ electrodes with different IrO_2 deposition charges. It is obvious that the sample electrode with a deposition charge of 500 mC has a higher porosity, which means that the surface structure formed under this condition is most prone to proton exchange.

3.6. Chronoamperometry study

Chronoamperometry was employed to study the stability of the $\text{IrO}_2/\text{TNTs}/\text{Ti}$ electrodes under the condition of oxygen evolution. The applied potential was 1.5 V, and the test temperature was $40\text{ }^\circ\text{C}$. According to the chronoamperometric curves in Fig. 9, there is a current drop at the initial stage, which

is due to the irregular dissolution of active substances at the edge of the electrode and the delayed electrolyte diffusion between the electrode surface and the solution under a high oxygen evolution overpotential [31,32]. The oxygen evolution current tends to be steady as the electrolysis process proceeds. The currents of the IrO₂/TNTs/Ti electrodes in the stabilized stage increase with increasing deposition charge. From the chronoamperometric curves of the IrO₂/TNTs/Ti electrodes prepared at different calcination temperatures, it can be seen that the electrode calcined at 450 °C has a higher steady current, which means a better catalytic activity and stability. When the calcination temperature reaches 550 °C or above, the oxygen evolution current is almost negligible, showing poor catalytic properties.

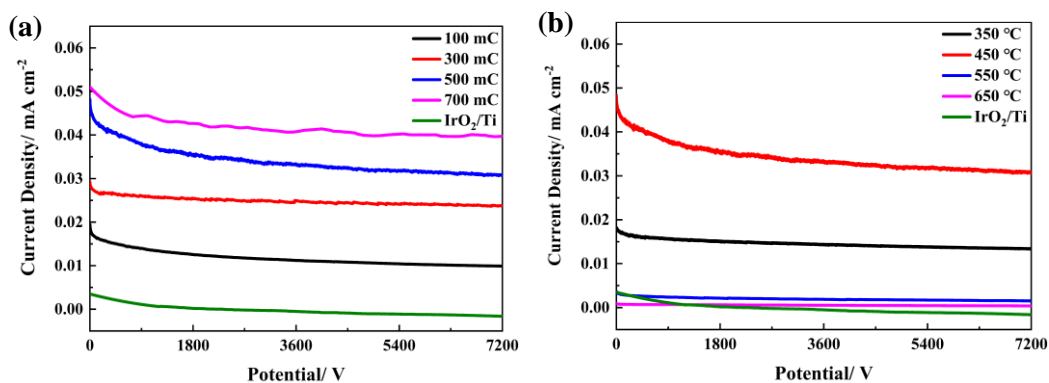


Figure 9. Chronoamperometric plots of the IrO₂/Ti and IrO₂/TNTs/Ti electrodes with (a) different IrO₂ deposition charges (calcination temperature: 450 °C) and (b) different calcination temperatures (deposition charge: 500 mC) in 1 mol L⁻¹ H₂SO₄ (potential: 1.5 V; test temperature: 40 °C).

4. CONCLUSION

In summary, TNTs-mediated IrO₂ active anodes were successfully fabricated by an electrodeposition and heat treatment process. The nanostructure of the TNTs provides a beneficial spatial structure for the growth of active IrO₂, which ensures the desired electrocatalytic activity and adaptability of an electrode for long-term use in the OER. The electrochemical surface structure of this novel OER anode was revealed by cyclic voltammetry studies. Both the "external" and the "internal" active sites could well exert their effects when the deposition charge of IrO₂ was controlled at 500 mC, and a higher porosity was obtained in this case, which means that the surface structure formed under this condition is the most prone to proton exchange. The calcination temperature is particularly important for this nanostructured electrode. The IrO₂/TNTs/Ti electrode calcined at 450 °C has a higher steady current, while the oxygen evolution current is almost negligible for the sample electrode calcined at 550 °C or above, which is largely due to the destruction of the electrode nanostructure at higher temperatures.

ACKNOWLEDGMENTS

This work was supported by the Natural Science Foundation of Zhejiang Province (No. LY17B030009).

References

1. C. Liu, R. Röder, L. Zhang, Z. Ren, H. Chen, Z. Zhang, C. Ronning and P.X. Gao, *J. Mater. Chem.*

- A, 2 (2014) 4157.
2. D.C. Nguyen, T.L.L. Doan, S. Prabhakaran, D.T. Tran, D.H. Kim, J.H. Lee and N.H. Kim, *Nano Energy*, 82 (2021) 105750.
 3. Y. Duan, Z.Y. Yu, S.J. Hu, X.S. Zheng, C.T. Zhang, H.H. Ding, B.C. Hu, Q.Q. Fu, Z.L. Yu, X. Zheng, J.F. Zhu, M.R. Gao and S.H. Yu, *Angew. Chem. Int. Ed.*, 58 (2019) 15772.
 4. M.T.M. Koper, *J. Electroanal. Chem.*, 660 (2011) 254.
 5. N.T. Suen, S.F. Hung, Q. Quan, N. Zhang, Y.J. Xu and H.M. Chen, *Chem. Soc. Rev.*, 46 (2017) 337.
 6. L.M. Gajić-Krstajić, T.L. Trišović and N.V. Krstajić, *Corros. Sci.*, 46 (2004) 65.
 7. Z.X. Lu, Y. Shi, C.F. Yan, C.Q. Guo and Z.D. Wang, *Int. J. Hydrogen Energy*, 42 (2017) 3572.
 8. X.M. Chen, G.H. Chen and P.L. Yue, *J. Phys. Chem. B*, 105 (2001) 4623.
 9. J.C. Cruz, V. Baglio, S. Siracusano, R. Ornelas, L. Ortiz-Frade, L.G. Arriaga, V. Antonucci and A.S. Aricò, *J. Nanopart. Res.*, 13 (2010) 1639.
 10. J. Ahmed and Y. Mao, *Electrochim. Acta*, 212 (2016) 686.
 11. R.M. Belal, M.A. Zayed, R.M. El-Sherif and N.A.A. Ghany, *J. Electroanal. Chem.*, 882 (2021) 114979.
 12. R. Ma, S. Cheng, X. Zhang, S. Li, Z. Liu and X. Li, *Hydrometallurgy*, 159 (2016) 6.
 13. I. Ivanov, Y. Stefanov, Z. Noncheva, M. Petrova, Ts. Dobrev, L. Mirkova, R. Vermeersch and J.P. Demaerel, *Hydrometallurgy*, 57 (2000) 125.
 14. R.A. Herrada, S.E. Rodil, S. Sepúlveda-Guzmán, J. Manríquez, K.S. Exner and E. Bustos, *J. Alloys Compd.*, 862 (2021) 108015.
 15. A. Ali, M. Shoeb, Y. Li, B. Li and M.A. Khan, *J. Mol. Liq.*, 324 (2021) 114696.
 16. H.Y. Yang, S.H. Lee, H.M. Kim, X.H. Pham, E. Hahm, E.J. Kang, T.H. Kim, Y. Ha, B.H. Jun and W.Y. Rho, *J. Ind. Eng. Chem.*, 80 (2019) 311.
 17. B. Zhang, S. Sun, N. Shi, X. Liao, G. Yin, Z. Huang, X. Chen and X. Pu, *J. Alloys Compd.*, 820 (2020) 153066.
 18. C. Lu, L. Zhang, Y. Zhang and S. Liu, *Mater. Lett.*, 185 (2016) 342.
 19. A.K. Ayal, Z. Zainal, A.M. Holi, H.N. Lim, Z.A. Talib and Y.C. Lim, *J. Phys. Chem. Solids*, 153 (2021) 110006.
 20. D. Ning, A. Zhang, M. Murtaza and H. Wu, *J. Alloys Compd.*, 777 (2019) 1245.
 21. J. Xu, Y. Ao, M. Chen and D. Fu, *Appl. Surf. Sci.*, 256 (2010) 4397.
 22. M. Mehdipour, S.H. Tabaian and S. Firoozi, *Ceram. Int.*, 45 (2019) 19971.
 23. E. Binetti, Z. El Koura, N. Patel, A. Dashora and A. Miotello, *Appl. Catal., A*, 500 (2015) 69.
 24. R.V. Genova-Koleva, F. Alcaide, G. Álvarez, P.L. Cabot, H.J. Grande, M.V. Martínez-Huerta and O. Miguel, *J. Energy Chem.*, 34 (2019) 227.
 25. W. Hu, S.L. Chen and Q.H. Xia, *Int. J. Hydrogen Energy*, 39 (2014) 6967.
 26. Y. Liu, C. Wang, Y. Lei, F. Liu, B. Tian and J. Wang, *Int. J. Hydrogen Energy*, 43 (2018) 19460.
 27. Y. Li, Q. Ma, J. Han, L. Ji, J. Wang, J. Chen and Y. Wang, *Appl. Surf. Sci.*, 297 (2014) 103.
 28. S. Trasatti, *Electrochim. Acta*, 36 (1991) 225.
 29. C.P. De Pauli and S. Trasatti, *J. Electroanal. Chem.*, 396 (1995) 161.
 30. S. Ardizzone, G. Fregonara and S. Trasatti, *Electrochim. Acta*, 35 (1990) 263
 31. K. Kadakia, M.K. Datta, O.I. Velikokhatnyi, P. Jampani, S.K. Park, S.J. Chung and P.N. Kumta, *J. Power Sources*, 245 (2014) 362.
 32. K. Kadakia, M.K. Datta, P.H. Jampani, S.K. Park and P.N. Kumta, *J. Power Sources*, 222 (2013) 313.